Generation of Electricity Hot Paper

DOI: 10.1002/anie.201309029

Induction of Electromotive Force by an Autonomously Moving Magnetic Bot**

*Sunil Kumar Sailapu and Arun Chattopadhyay**

Abstract: *We report the observation of the induction of electromotive force (emf) into a Faraday coil by an autonomously moving composite magnetic particle in aqueous medium. The particle consisted of a micron-sized polymer sphere, which was decorated with catalytic Pd nanoparticles (NPs) and attached to a micron-scale (N-42 grade) rare-earth magnet. The Pd NPs catalytically decomposed H_2O_2 to generate O_2, resulting in buoyancy-driven vertical motion of the particle, while the micromagnet induced emf during the flight. Because a small volume of ethanol was layered on top of the liquid, the bubble burst when the particle ascended to the top and thus nearly continuous vertical motion was achieved. Spikes of alternating electrical signal could be observed up to 20 times per minute. The signal was sufficiently strong to illuminate light-emitting diodes following appropriate amplification. This distinctive approach is expected to pave the way to developing synthetic bots which are autonomously propelled, generating their own signal for running complex circuitry.*

The advent of nanoscale science and technology has kindled vigorous interest in the systematic development in the field of the autonomous motion of microscopic objects in liquid media.[1,2] Significant developments have been based on the use of the catalytic decomposition of H_2O_2 and the nanoscale manipulation of biomolecules in moving objects of micron-scale and nanoscale dimensions. Bubble propulsion,[3–5] electrophoresis,[6] thermophoresis,[7] diffusiophoresis,[8] magnetophoresis,[9] and motion due to interfacial gradients[10] are the primary mechanisms forming the basis of motion of these objects. Control over the motion has been achieved by external magnetic fields,[11] thermal modulations,[12–14] light,[15] ultrasonic waves,[16] internal pH[17] and chemical gradients,[18] viscosity of the medium,[19] and surface tension[20] of the liquid. Further, nanoscale motors based on organic molecules[21] and DNA[22] offer the option of specific functionalization and thereby molecular control over their properties and motion. Essentially, the efforts have been to emulate the function of naturally occurring biological nanoscale motors[23,24]—at least partially—by using chemical energy as the driving force for the motion. Although there have been reports of using this motion to achieve model-targeted drug delivery,[25] there is no report of using the motion of the nanoscale objects as a useful source of secondary energy. For example, it is conceivable that the production of electrical energy in situ would make it possible for the nanobots not only to display controlled motion but also to perform higher level functions for which the required additional energy may not be available or achievable using conventional bots. Thus an autonomously moving magnetic device could generate electrical energy induced by its motion through a metallic or otherwise electrically conducting coil. This could also pave the way for communicative bots. However, the possibility of such a transduction needs to be demonstrated first.

Herein we report the induction of electromotive force (emf) into a Faraday coil by an autonomously moving magnetic microparticle which was attached to a polymer resin containing catalytic Pd nanoparticles (NPs). The catalytic decomposition of aqueous H_2O_2 generated O_2 bubbles which were adsorbed on the microbot resulting in buoyancy-driven vertical motion of the attached magnet. Alternating electrical signals were generated about 20 times per minute for the vertical flights up and down a glass tube. The signal strength could also be improved to be sufficiently strong for amplification to light an LED, when a larger magnet was used. The experimental design also allowed for periodic vertical motion of the bot until the fuel was exhausted.

Figure 1 shows the overall experimental setup and the resultant emf generated by the vertical motion of the microbot. Driven by the catalytic decomposition of hydrogen peroxide (fuel), the bot marked a thermodynamic efficiency of 8.7×10^{-5}% (see Reaction Kinetics and Efficiency Calculations in the Supporting Information), which is generally higher than the efficiencies calculated for fuel-driven propulsion.[26]

The microbot was made of two components: Pd NPs embedded in a micron-sized polymer resin sphere and a micron-sized (N-42 grade) rare-earth magnet which was affixed to the polymer. The overall diameter of the object was 1.4 mm (Figure 1b). The fabrication of the bot is detailed in the Experimental Section. The bot was placed in a Borosil glass tube which was wrapped with copper wire (34 SWG, 1000 windings) as shown in Figure 1a. The glass tube was filled with 1 mL of 5% (w/v) aqueous H_2O_2. The Pd NPs catalyzed the decomposition of H_2O_2 into O_2; the so-

[*] S. K. Sailapu, Prof. A. Chattopadhyay
Centre for Nanotechnology
Indian Institute of Technology Guwahati
Guwahati, Assam (India)
Prof. A. Chattopadhyay
Department of Chemistry
Indian Institute of Technology Guwahati
Guwahati, Assam (India)
E-mail: arun@iitg.ernet.in

[**] We thank the Department of Biotechnology, Government of India for funding. We thank the Central Instrument Facility, IITG, and Dr. Chivukula V. Sastri, Dr. Krishna Kanti Dey, Chandan Borgohain, Satyapriya Bhandari, Ashoka Vardhan Botta, Narendra Allu, Chanikya Gorapalli, and Ravi Kiran Anjani for their help.

Supporting information for this article is available on the WWW under http://dx.doi.org/10.1002/anie.201309029.

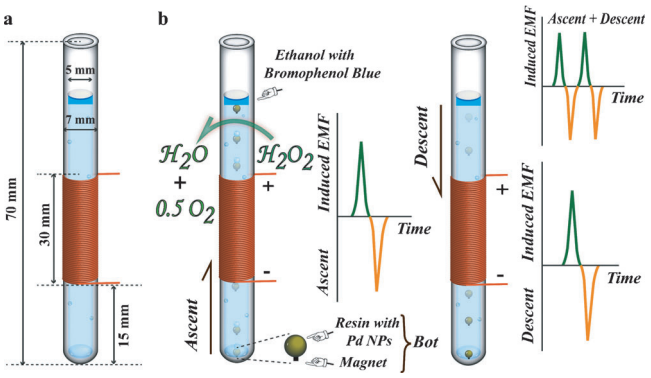

Figure 1. Experimental design. a) In the experiment a glass tube contains 1 mL of 5% aqueous H_2O_2, along with 60 µL of ethanol (mixed with bromophenol blue) layered on the top. A part of the tube was wrapped with a copper coil (red) for emf induction. b) The bot, which is a resin bead containing embedded Pd nanoparticles with an attached rare-earth magnet, was placed at the bottom of the tube. Left tube: Pd-catalyzed decomposition of H_2O_2 generates O_2, which forms bubbles providing buoyancy for the upward motion of the bot. Right tube: The bubbles burst when the bot comes in contact with ethanol, making the bot descend. Each flight (ascent and descent) generates an emf signal as shown in the plots beside the tubes. The overall signal for one cycle is shown on top right.

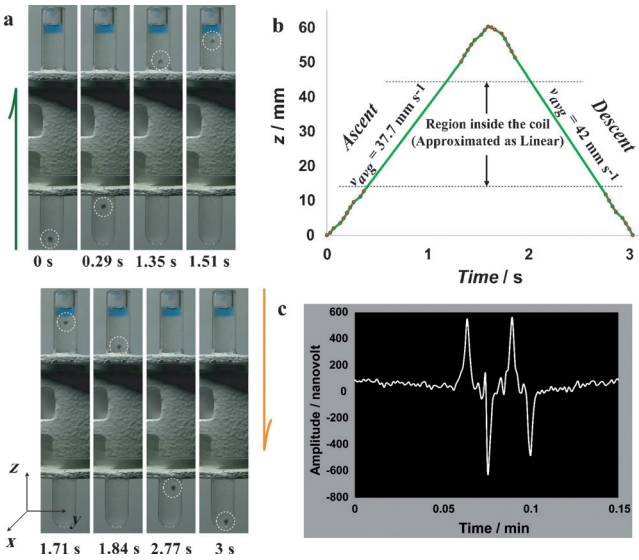

Figure 2. Motion profile of the bot and induced voltage. a) Frame-by-frame images showing the ascending (top) and descending (bottom) phases of the bot. b) Position versus time plot of the ascent and the descent phases with average velocity in each phase. c) Plot illustrates the induced voltage resulting from one cycle of the autonomous motion of the bot.

produced oxygen bubbles adhered to the polymer bead and eventually a single larger bubble formed by coalescence of several smaller bubbles.[11,19] When the number of bubbles or the total volume of the bubble was sufficiently high, then the buoyancy force balanced the gravitational and viscous forces on the bot and the bead moved upward with terminal velocity[11] (ascent phase in Figure 1b). It may be mentioned here that when the bot was made of only the magnet, then the H_2O_2 decomposition rate was significantly small and thus the rate of bubble growth was very slow (Supporting Information, Movie S1, Figure S1).

Incorporation of Pd NPs embedded polymer sphere led to faster bubble formation and hence this construction was preferred. Further, it was observed that the bot remained stationary at the meniscus for a sufficiently long time or moved to the wall of the tube, due to the attached bubbles and a rapid downward movement was prevented (descent phase in Figure 1b). This was addressed by layering 60 µL of ethyl alcohol (95% v/v)—a known bubble breaker[27]—mixed with bromophenol blue on the top of the reaction liquid (Figure 1). We used bromophenol blue as we could observe and record the stability of the alcohol layer and it did not participate in any reaction. Thus the experimental arrangement allowed the repeated vertical motion of the microbot with a frequency of about five cycles per minute.

Figure 2a shows images of the microbot at different vertical positions during its motion for a complete cycle. As is clear from the images, the bot stayed away from the wall and moved through nearly the center of the liquid column during its flight. It is important to mention here that the average velocity of the bot during its upward movement was 37.7 mm s^{-1} and for the downward movement it was 42 mm s^{-1}; this corresponds to 27 and 30 times its body length per second as inferred from the motion profile in Figure 2b. Further, as the magnetic chemical locomotor moved up and down, its magnetic flux induced emf into the surrounding copper coil. The electrical signal appeared in the form of spikes with a magnitude on the order of nanovolts for each direction of motion. A typical voltage output profile for one cycle of motion is shown in Figure 2c. Thus when the magnetic bot approaches the coil from one end of the tube, an induced signal is generated in response to the change in magnetic flux. Also, when the bot comes out of the coil from the other end, the flux alters again, inducing another signal but with opposite polarity (also shown schematically in Figure 1b).

For one cycle of motion (Supporting Information, Movie S2) four signal spikes could be observed, two corresponding to the ascent phase and other two corresponding to the descent phase (Figure 2c). For an observation period of 20 min (Figure 3), the bot cycled with an average frequency of five times per min (Supporting Information, Figure S2). As the number of windings in the copper coil was fixed, the variation in the amplitudes of the voltages can only be attributed to the rate of change of flux through the coil as the bot is propelled. The periodicity, reproducibility of motion of the bot, and corresponding electrical signal generation are clearly supported by the observed results (Figures 2 and 3). It is worth mentioning here that the signal was much higher than the noise and significant spikes were generated only when the bot was in motion. Further, when the concentration of H_2O_2 was changed there was no discernible effect on the velocity, since the bot achieved terminal velocity when the buoyant force was balanced by the gravitational and viscous forces.[11] However, the number of times the bot moved up and down changed. At low H_2O_2 concentration (2%) the rate was low (1–2 cycles per min), while it was high (5 cycles per min) at higher concentration (5%).

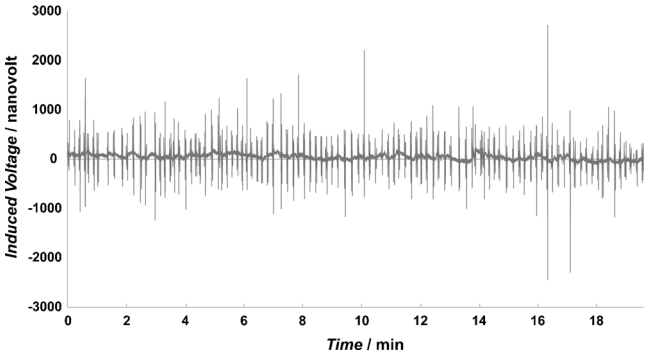

Figure 3. Signal generated from autonomous motion. Induced voltage generated from the motion of the bot for a period of about 20 min. The spikes denote the signal observed during the flight of the bot.

In order to account for the shape and magnitude of the observed emf, first of all it is important to have a clear picture of the average velocity and path of the bot. An analysis of the motion of the bot (Figure 2b) indicates that the locomotor moves with nearly constant velocity. Also, the path of the bot is nearly vertical in both its upward and downward journeys. The motion profile linked with the induced voltage is theoretically modeled (Figure 4) under certain assumptions. These assumptions include that the force resulting from the capillary pressure inside the bubble ($\mathbf{F_p}$) balances the capillary force ($\mathbf{F_c}$).[19] The magnet is assumed to be a perfect dipole. The fluid is considered incompressible and the drag forces to be governed by Stokes law. The buoyancy force $\mathbf{F_b}$, the gravitational force $\mathbf{F_g}$ and the drag force $\mathbf{F_d}$ together largely account for the dynamics of the bot as depicted in the Figure 4a. To simplify the calculation, the coil is assumed to be moving and the bot is kept in a fixed position; this does not alter the problem to be addressed. The spatial (Figure 4b) and temporal patterns (Figure 4c) of the signal as it crosses the origin are of alternating type. The theoretical model predicts the same type of signal as that observed in the experiments. Moreover, the signal shape, being associated with the coil radius, also depends upon the distance the bot travels after crossing the coil (Figure 4b). Needless to mention, only changes in fluxes through the coil would result in the generation of signal, that is, when the bot is in motion (Theoretical Deductions in the Supporting Information). Also, the faster the motion of the bot in linear direction with no change in orientation, the shorter the time period and the stronger the signal (Figure 4c). Further, if the orientation of the bot changes during the flight, it affects the rate of change of flux through the coil accordingly, resulting in the generation of a signal with corresponding strength and polarity. The model depicted here clearly shows possible variations with alterations in the basic parameters. It was not possible to obtain quantitative results since the variations in fluxes were too small to be measured.

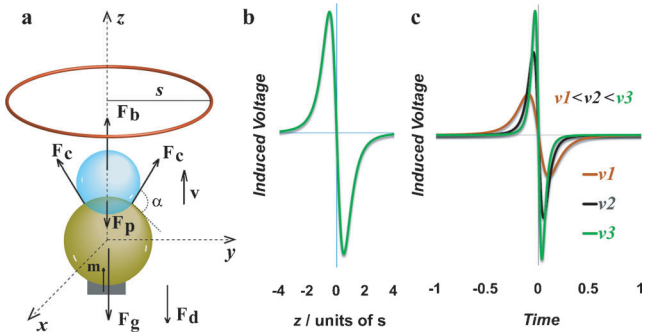

Figure 4. a) Theoretical model showing the various forces acting on the system. Here $\mathbf{F_b}$, $\mathbf{F_g}$, and $\mathbf{F_d}$ represent the buoyancy, gravitational, and drag forces, respectively. $\mathbf{F_c}$ is the capillary force and and $\mathbf{F_p}$ is the force resulting due to capillary pressure inside the bubble. Magnetic moment and the radius of the coil are denoted by **m** and *s*, respectively. b) Spatial plot: Induced voltage generated as function of position, when the bot moves in and out of the static coil. Here, 'z' is taken in units of 's', where 's' is the radius of the coil. c) Temporal plot**:** Induced voltage plotted with the variations in velocity clearly indicates that as the velocity increases, the amplitude rises with the decrease in time span. Here, origin is taken as the time when the polarity of the signal alters.

It is interesting to gauge the quality of the electrical signal generated by the motion of the bot. In order to illustrate this, LEDs were incorporated in the circuit with appropriate amplifiers for boosting the signal (see Circuit Design in the Supporting Information). The magnet used was a cube with sides measuring 900 microns . The motion and simultaneous voltage generation could be captured alongside the lighting of the LEDs (green and orange) on the upward and downward flights of the bot (Supporting Information, Movie S3, Figure S3). This shows that the bot can perform secondary actions as a result of its motion and thus it may be possible to introduce versatility in a more complex system.

In the quest for developing an autonomously moving bot with secondary function, a new function, namely production of electrical energy, was achieved using a composite system. Thus, while the catalytic Pd NPs present in the polymer microsphere generated oxygen needed for the motion of the bot, the magnetic component induced emf into a coil connected to an electrical circuit. The periodicity and reproducibility of the vertical motion and generation of electrical current of sufficient magnitude for lighting LEDs during the course of the motion indicate favorable prospects for the design of multifunctional autonomous microscopic bots. The generation of an electrical signal could be accounted for using a conventional Faradaic model and this promotes the possible incorporation of low-voltage operating devices in autonomously moving electrically operative microbots.

Experimental Section

Design and characterization of the bot: Preparation of Pd NPs on micron-sized beads involved, firstly, activation of highly stable polymer spheres (3 g, polystyrene divinylbenzene copolymer, Amberlite-IR 120, Merck) by placing them in HCl (10 mL, 3 M, Merck) for an hour. After thorough washing with Milli Q grade water, the cation-exchange beads were transferred to a solution containing H_2PdCl_4 (5 mL, 0.2 M, Sigma–Aldrich) and they were then left for three hours in order to exchange Pd^{2+}. The beads were washed with water and then treated with $NaBH_4$ (5 mL, 10 mM, Merck), which was added slowly with stirring for 2 h. They were washed with water again and then air dried. Visual examination (Supporting Information, Fig-

ure S5a) of the control and the coated particles gave the first signs of the formation of Pd NPs on the polymer. X-ray diffraction experiments were performed for further examination (Supporting Information, Figure S5b). The formation of particles was confirmed using electron microscopic analysis (Supporting Information, Figures S6 and S7). The resulting Pd NPs were small with a mean size of (9.4 ± 5.9) nm, based on transmission electron microscopy, making those good candidates for catalysis. An extracted small fragment of a N-42 grade magnet was affixed to this NP-coated microsphere using epoxy adhesive. The fragment of the magnet (Supporting Information, Figure S8) used for the experiment was characterized in order to confirm its salient properties.

The design of the autonomous triggering device and the autonomous signal generator are detailed at the end of Supporting Information in the Additional Experimental Details.

Received: October 16, 2013
Published online: January 21, 2014

Keywords: autonomous motion · electromotive force · heterogeneous catalysis · hydrogen peroxide · palladium

[1] G. A. Ozin, I. Manners, S. Fournier-Bidoz, A. Arsenault, *Adv. Mater.* **2005**, *17*, 3011 – 3018.
[2] C. R. Lowe, *Curr. Opin. Struct. Biol.* **2000**, *10*, 428 – 434.
[3] Y. Wu, Z. Wu, X. Lin, Q. He, J. Li, *ACS Nano* **2012**, *6*, 10910 – 10916.
[4] S. Sanchez, A. A. Solovev, S. M. Harazim, O. G. Schmidt, *J. Am. Chem. Soc.* **2011**, *133*, 701 – 703.
[5] J. G. Gibbs, Y. P. Zhao, *Appl. Phys. Lett.* **2009**, *94*, 163104.
[6] R. Liu, A. Sen, *J. Am. Chem. Soc.* **2011**, *133*, 20064 – 20067.
[7] L. Ionov, M. Stamm, S. Diez, *Nano Lett.* **2006**, *6*, 1982 – 1987.
[8] M. E. Ibele, P. E. Lammert, V. H. Crespi, A. Sen, *ACS Nano* **2010**, *4*, 4845 – 4851.
[9] L. Baraban, D. Makarov, O. G. Schmidt, G. Cuniberti, P. Leiderer, A. Erbe, *Nanoscale* **2013**, *5*, 1332 – 1336.
[10] W. F. Paxton, K. C. Kistler, C. C. Olmeda, A. Sen, S. K. St. Angelo, Y. Cao, T. E. Mallouk, P. E. Lammert, V. H. Crespi, *J. Am. Chem. Soc.* **2004**, *126*, 13424 – 13431.
[11] K. K. Dey, D. Sharma, S. Basu, A. Chattopadhyay, *J. Chem. Phys.* **2008**, *129*, 121101 – 121104.
[12] S. Balasubramanian, D. Kagan, K. M. Manesh, P. Calvo-Marzal, G.-U. Flechsig, J. Wang, *Small* **2009**, *5*, 1569 – 1574.
[13] S. Sanchez, A. N. Ananth, V. M. Fomin, M. Viehrig, O. G. Schmidt, *J. Am. Chem. Soc.* **2011**, *133*, 14860 – 14863.
[14] L. Soler, C. Martinez-Cisneros, A. Swiersy, S. Sanchez, O. G. Schmidt, *Lab Chip* **2013**, *13*, 4299 – 4303.
[15] V. Balzani, M. Clemente-León, A. Credi, B. Ferrer, M. Venturi, A. H. Flood, J. F. Stoddart, *Proc. Natl. Acad. Sci. USA* **2006**, *103*, 1178 – 1183.
[16] W. Wang, L. A. Castro, M. Hoyos, T. E. Mallouk, *ACS Nano* **2012**, *6*, 6122 – 6132.
[17] K. K. Dey, S. Bhandari, D. Bandyopadhyay, S. Basu, A. Chattopadhyay, *Small* **2013**, *9*, 1916 – 1920.
[18] L. Baraban, S. M. Harazim, S. Sanchez, O. G. Schmidt, *Angew. Chem.* **2013**, *125*, 5662 – 5666; *Angew. Chem. Int. Ed.* **2013**, *52*, 5552 – 5556.
[19] A. Agrawal, K. K. Dey, A. Paul, S. Basu, A. Chattopadhyay, *J. Phys. Chem. C* **2008**, *112*, 2797 – 2801.
[20] L. Courbin, F. Artzner, *Nat. Mater.* **2012**, *11*, 1008 – 1009.
[21] D. A. Wilson, R. J. M. Nolte, J. C. M. van Hest, *Nat. Chem.* **2012**, *4*, 268 – 274.
[22] Y. Chen, M. Wang, C. Mao, *Angew. Chem.* **2004**, *116*, 3638 – 3641; *Angew. Chem. Int. Ed.* **2004**, *43*, 3554 – 3557.
[23] E. S. Russell, *Nature* **1941**, *147*, 190 – 191.
[24] H. C. Berg, *Nature* **1975**, *254*, 389 – 392.
[25] Z. Wu, Y. Wu, W. He, X. Lin, J. Sun, Q. He, *Angew. Chem.* **2013**, *125*, 7138 – 7141; *Angew. Chem. Int. Ed.* **2013**, *52*, 7000 – 7003.
[26] W. Wang, T.-Y. Chiang, D. Velegol, T. E. Mallouk, *J. Am. Chem. Soc.* **2013**, *135*, 10557 – 10565.
[27] K. Cho, S. Chida, M. Sasaki, T. Fujiwara, *Acta Paediatr. Jpn.* **1996**, *38*, 322 – 327.

